Evaluation of Stimulated Raman Scattering Microscopy for Identifying Squamous Cell Carcinoma in Human Skin

Richa Mittal, MS,[1,2] Mihaela Balu, PhD,[1] Tatiana Krasieva, PhD,[1] Eric O. Potma, PhD,[1,3] Laila Elkeeb, MD,[4] Christopher B. Zachary, MBBS, FRCP,[4] and Petra Wilder-Smith, DDS, PhD[1]*

[1]*Beckman Laser Institute and Medical Clinic, University of California, Irvine, California 92612*

[2]*Department of Chemical Engineering and Materials Sciences, University of California, Irvine, California 92697*

[3]*Department of Chemistry, University of California, Irvine, California 92697*

[4]*Department of Dermatology, University of California, Irvine, California 92697*

Background and Significance: There is a need to develop non-invasive diagnostic tools to achieve early and accurate detection of skin cancer in a non-surgical manner. In this study, we evaluate the capability of stimulated Raman scattering (SRS) microscopy, a potentially non-invasive optical imaging technique, for identifying the pathological features of s squamous cell carcinoma (SCC) tissue.

Study design: We studied *ex vivo* SCC and healthy skin tissues using SRS microscopy, and compared the SRS contrast with the contrast obtained in reflectance confocal microscopy (RCM) and standard histology.

Results and Conclusion: SRS images obtained at the carbon-hydrogen stretching vibration at $2945\,cm^{-1}$ exhibit contrast related protein density that clearly delineates the cell nucleus from the cell cytoplasm. The morphological features of SCC tumor seen in the SRS images show excellent correlation with the diagnostic features identified by histological examination. Additionally, SRS exhibits enhanced cellular contrast in comparison to that seen in confocal microscopy. In conclusion, SRS represents an attractive approach for generating protein density maps with contrast that closely resembles histopathological contrast of SCC in human skin. Lasers Surg. Med. © 2013 Wiley Periodicals, Inc.

Key words: skin cancer; squamous cell carcinoma; stimulated Raman scattering; confocal reflectance microscopy; optical microscopy

INTRODUCTION

Optical microscopy studies of skin cancer, the most common form of cancer, have been facilitated by the manifestation of the disease in superficial tissue layers that are easily accessible for optical inspection. Due to the optical accessibility of the epidermis, skin cancer is often used as a model for evaluating novel diagnostic and therapeutic approaches. While the majority of skin carcinoma lesions are in the form of a basal cell carcinoma (BCC), squamous cell carcinoma (SCC) is the second most common pathology, constituting 20% of all cutaneous malignancies [1]. SCC is a malignant tumor arising from uncontrolled growth of epithelial keratinocytes. It is estimated that 700,000 cases of SCC are diagnosed annually in the US, resulting in approximately 2,500 deaths [2,3]. Although most of the non-melanoma skin cancer cases can be cured, rising incidence and local invasiveness constitute an important clinical challenge. Today, non-melanoma skin cancer is diagnosed by visual inspection followed by invasive skin biopsy and histopathlogical examination. Patients with SCC are at an increased risk of future SCC tumor development, especially in the same location or surrounding tissue. Primary cutaneous SCCs can metastasize unless treated early by optimal surgical techniques, and thus early diagnosis is important. While clinical diagnosis is generally quite accurate, these suspicious lesions are currently diagnosed by an invasive biopsy and sent for histopathological examination. Given the advances in optical diagnostic devices, there exists a need to develop non-invasive diagnostic tools to achieve early and accurate detection in a non-surgical manner, along with the ability to monitor these at-risk sites of field cancerization.

In the past decade, a number of non-invasive diagnostic methods have been studied for the skin including dermoscopy, high frequency ultrasound, optical coherence tomography (OCT), reflectance confocal microscopy (RCM), and multiphoton microscopy. Dermoscopy is routinely used in the clinical setting and its capability to

identify SCC *in situ* [4], pigmented BCCs and atypical melanocytic lesions has been demonstrated [5]. However, dermoscopy provides insufficient resolution to resolve important diagnostic and prognostic cellular details. OCT studies have identified features of BCC [6] and actinic keratosis (AK) [7] up to depths of 0.5–1.0 mm, however, due to the limited resolution capabilities of OCT, cellular, and subcellular features are not readily discernible in these images. Confocal microscopy on the other hand, has shown to be capable of resolving cellular and subcellular details, both with reflectance contrast *in vivo* [8–11] and with contrast agents *ex vivo* [11–16]. These high resolution optical microscopy techniques [17,18] have the greatest potential for clinical acceptance given their ability to visualize cellular structures and in reality performing an *in-vivo* biopsy with all the advantages of immediacy, non-invasiveness, and patient acceptability.

Stimulated Raman scattering (SRS) is a non-linear optical microscopy technique which probes the vibrational signature of a molecule [19,20]. Unlike fluorescence imaging which probes exogenous or endogenous fluorophores, the SRS imaging provides label-free contrast that can be used to visualize specific molecular compounds based on their vibrational spectroscopic properties. Among the accessible vibrational modes, the carbon-hydrogen (CH) vibrational stretching plays an important role in SRS microscopy, because of the ubiquitous presence of CH moieties and the relatively high Raman cross sections of the corresponding modes. A variety of CH stretching modes, including CH_3 (methyl), CH_2 (methylene), and CH (methine) groups, produce strong vibrational band structures in the 2,700 and 3,100 cm^{-1} spectrum region. The CH_3 mode contributes to the vibrational signal of the proteins and lipids, while CH_2 mode is dominant in aliphatic lipids and can be used to map out protein and lipid densities in biological tissue. It has recently been shown that SRS mapping of the CH_2 and CH_3 mode can provide contrast that is reminiscent of the contrast seen in hematoxylin and eosin (H&E) staining of excised tissue specimens [21]. These studies have opened doors toward the generation of "histopathology-like" images of superficial tissues *in vivo*, avoiding the need for invasive biopsies or the application of labeling agents.

One of the premier targets of the SRS technique is skin tissue. With penetration depths up to 0.5 mm, SRS microscopy holds promise as a diagnostic tool of skin carcinomas, which are present in the optically accessible epidermis layer of the tissue. The goal of this translational study was to investigate the capability of SRS imaging using contrast from lipids and proteins present in the skin to detect and characterize SCC tumor. SRS imaging data were compared with two standards (1) RCM, which is currently the most widely used non-invasive high-resolution optical imaging technique and (2) microscopy of H&E-stained tissue sections the gold standard in clinical practice. Whereas RCM has gained clinical acceptance, the SRS technique has not reached this level of clinical translation yet. In order for SRS to make a clinical impact, several hurdles have to be overcome. Among these is a clear
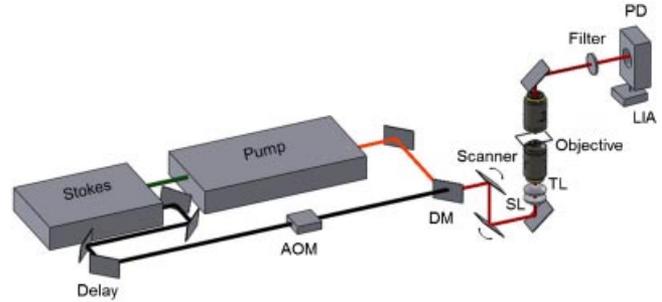

Fig. 1. Diagram delineating the components of the stimulated Raman scattering microscope set-up. AOM, acousto-optic modulator; DM, dichroic mirror; SL, scan lens; TL, tube lens; LIA, lock-in amplifier; PD, photodiode.

demonstration of meaningful diagnostic contrast for the case of SCC. In addition, a simple and robust imaging approach is required, which is compatible with real-time imaging applications in the clinic. In this work we use a rapid, simplified SRS approach for generating meaningful contrast, based on the direct mapping of the protein-like density of the methyl vibrational mode. This allows us to visualize the signal from proteins present in nuclei, cell membrane, and most abundant proteins in extracellular matrix-collagen, keratin. The signal thus acquired is compared with that seen in RCM. We conclude that SRS microscopy provides more cellular details and a more faithful representation of the tissue, which potentially could lead to a better diagnostic evaluation of skin cancers.

MATERIALS AND METHODS

Tissue Samples

Facial SCC and healthy skin tissue specimen were obtained per UCI IRB # 2008–6307. After excision through Mohs surgery the tissues were fixed in 2% paraformaldehyde in phosphate buffered (PBS) saline. Tissues were embedded in optimal cutting temperature (OCT) medium, snap frozen in liquid nitrogen and 20 μm thick sections were cut using a Microtome Cryostat HM 505E (MICROM, Walldorf, Germany). Tissue sections were placed on a glass microscope slide, immersed in PBS, and covered with a No. 1 borosilicate coverslip and sealed with epoxy glue. Unstained sectioned tissue was used for SRS imaging while the alternate tissue sections were stained with H&E for comparison. Experiments were performed at room temperature. Since the purpose of this study was to determine the SRS contrast from skin samples, we worked with sectioned tissue to enable optimum comparison with H&E and RCM imaging. It should be noted that in principle, SRS imaging could be extended to *in vivo* imaging without any need for tissue processing. This is dependent on the further development of an SRS fiber probe—an ongoing project in our lab.

Stimulated Raman Scattering (SRS) imaging

The SRS microscope uses an ultrafast light source that produces two beams, called pump and Stokes beams. The
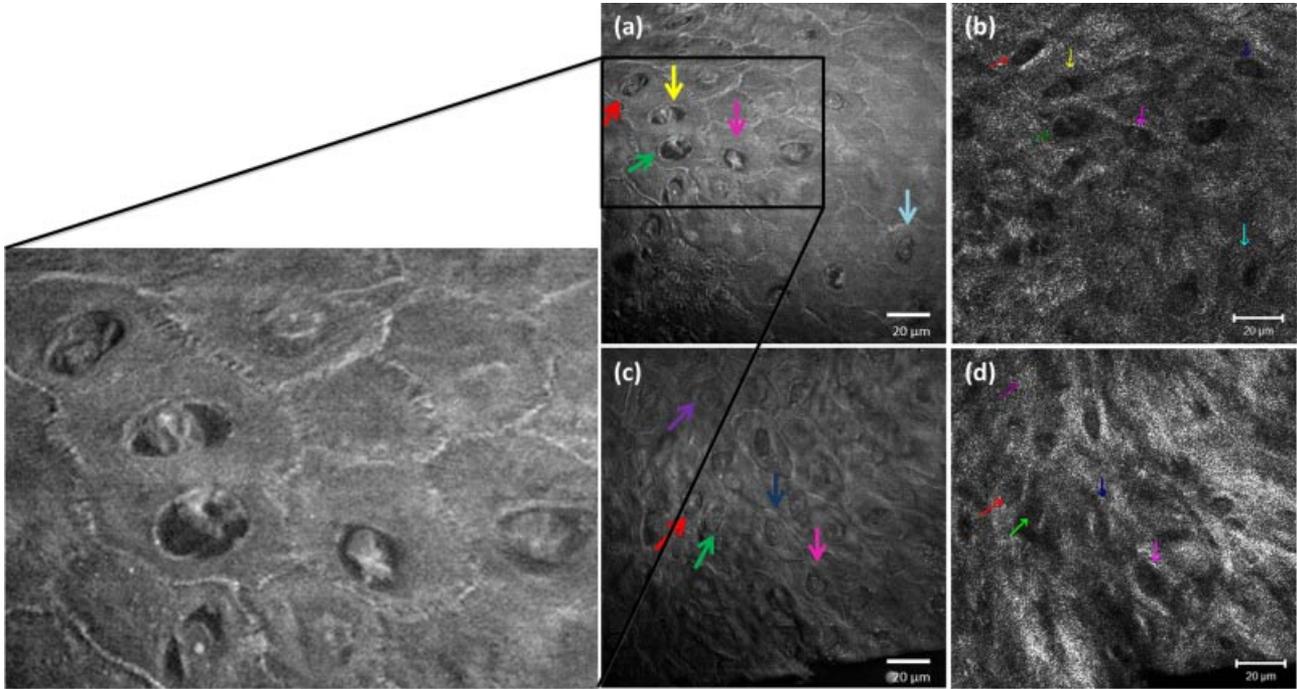
Fig. 2. Simultaneous comparison of SRS and RCM in SCC tumor. (**a**, **c**) SRS signal from keratinocytes imaged using 60X, 1.2 NA water objective, and simultaneously compared with the (**b**, **d**) respective confocal reflectance signal using 63X, 1.2 NA Apochromat water objective. On the left shows a magnified SRS image with enhanced cellular signal. The color coded arrows correspond to the same cells compared in both the techniques.

light source consists of an optical parametric oscillator (OPO; Levante Emerald, Berlin, Germany) pumped by a 7-ps, 76-MHz mode-locked Nd:vanadate laser (Picotrain; High-Q, Hohenems, Austria). The OPO tunable in the range of 800–820 nm was used as the pump beam in the SRS experiments. The Stokes beam was derived from the same 76-MHz Nd:vanadate laser fixed at 1,064 nm. The pump and Stokes beams were spatially and temporally overlapped on a dichroic mirror and sent into the galvanometer scanner (Fluoview 300; Olympus, Center Valley, PA), focusing the beam using a 20X, 0.75 NA objective Lens (UPlanSApo; Olympus) mounted on an inverted microscope (IX71; Olympus). For higher magnification a 60X, 1.2 NA water objective lens (UPlanSApo, Olympus) was used for comparison with the confocal images. To monitor stimulated Raman loss, the Stokes beam was modulated at 10 MHz with an acoustic optical modulator (Crystal Technology, Palo Alto, CA). The modulated pump intensity was detected by a photodiode (FDS1010; Thorlabs, Newton, NJ), and the signal was demodulated with a home-built lock-in amplifier. Figure 1 shows the different components in the SRS microscope. Scans were performed on each section of tissue with the frequency difference between beams tuned to the vibrational frequency $2,945 \text{ cm}^{-1}$. At this vibrational frequency, the signal obtained from the epidermis is dominated by a strong contribution from proteins, effectively generating a protein density map. To ensure sample integrity the

average combined power of pump and Stokes beam was kept under 30 mW at the sample.

Reflectance Confocal Imaging

A Zeiss LSM 510 Meta (Carl Zeiss AG, Oberkochen, Germany) laser scanning confocal microscope system was used for the confocal imaging experiments. The system is based on an Axiovert 200M inverted microscope and a helium: neon laser (543 nm) is used as a light source. The light beam is directed to the main dichroic beam splitter, which deflects the 543 nm excitation wavelength to the sample and transmits a portion of the reflected light. A narrow band pass filter (BP 500–550) and a pinhole in front of the photomultiplier tube detector are used to reject any potential fluorescence signal. The laser beam was focused through a 63X, 1.2 NA water-immersion objective (C-Apochromat; Zeiss, Jena, Germany) for comparison with SRS images. The illumination power at the sample was below 15 mW.

RESULTS

Comparison of SRS and RCM

Images from keratinocytes in SCC acquired with SRS microscopy are compared with images obtained with RCM imaging (Fig. 2). Higher magnification revealed the capabilities of the two imaging techniques. The presence of rounded cellular structures is evident using both

techniques. However, the enhanced SRS signal from the cell nuclei and the cell boundaries provide a markedly better cellular and nuclear detail than that obtained using RCM (Fig. 2a,c). Visualization of these features is important as they serve as staging markers for skin cancer progression. The various diagnostic criteria for neoplasia, especially the shape of cells and nuclei, the size of nuclei, and the nuclear-to-cytoplasm ratio can be assertively determined with SRS imaging. The nuclei of atypical cells are only visible using SRS imaging and they are not discernible with RCM contrast. Examination of cells and their nuclei is difficult in RCM because the cell nuclei lack signal relative to the cell cytoplasm (Fig. 2b,d).

Correlation of SRS with H&E Microscopy (Healthy and SCC Tissue)

A mosaic of SRS images of the skin sample (Fig. 3a,c) is compared with H&E stained histopathology section (Fig. 3b,d). The SRS image reveals all of the morphological features of the epidermis and dermis that are demarcated in the H&E stained section. The SRS signal in healthy skin (Fig. 3a) shows well-defined epithelium cellular layers and sub-epithelium with a strong protein signal from the extracellular matrix, imaged to an anatomical depth of $300\,\mu m$. On the contrary, in Figure 3c, the epidermis is revealing cup or finger like projections, extending deep into the dermis. While the neoplastic epithelium is pushing down into the dermis, the basement membrane is still intact (arrow marked in Fig. 3c). The large sized tumor was imaged down to 1.1 mm anatomical depth. The growth of the tumor cells is prevalent all over the tissue as similarly observed in H&E histopathology. The SRS images correlate well with the corresponding histopathology sections, reproducing "histopathology-like" features of cutaneous SCC.

Superficial SCC Features

Individual images were taken at different depths and higher magnification to observe various features in superficial SCC. SRS imaging of SCC tumor can characterize atypical keratinocytes with similar information content as seen in standard H&E histopathology as shown in Figure 4. These images correspond to the optical sections parallel to the surface of the skin tissue. Protein signals from the cell nuclei allow the visualization of general morphology such as different shapes and sizes of atypical
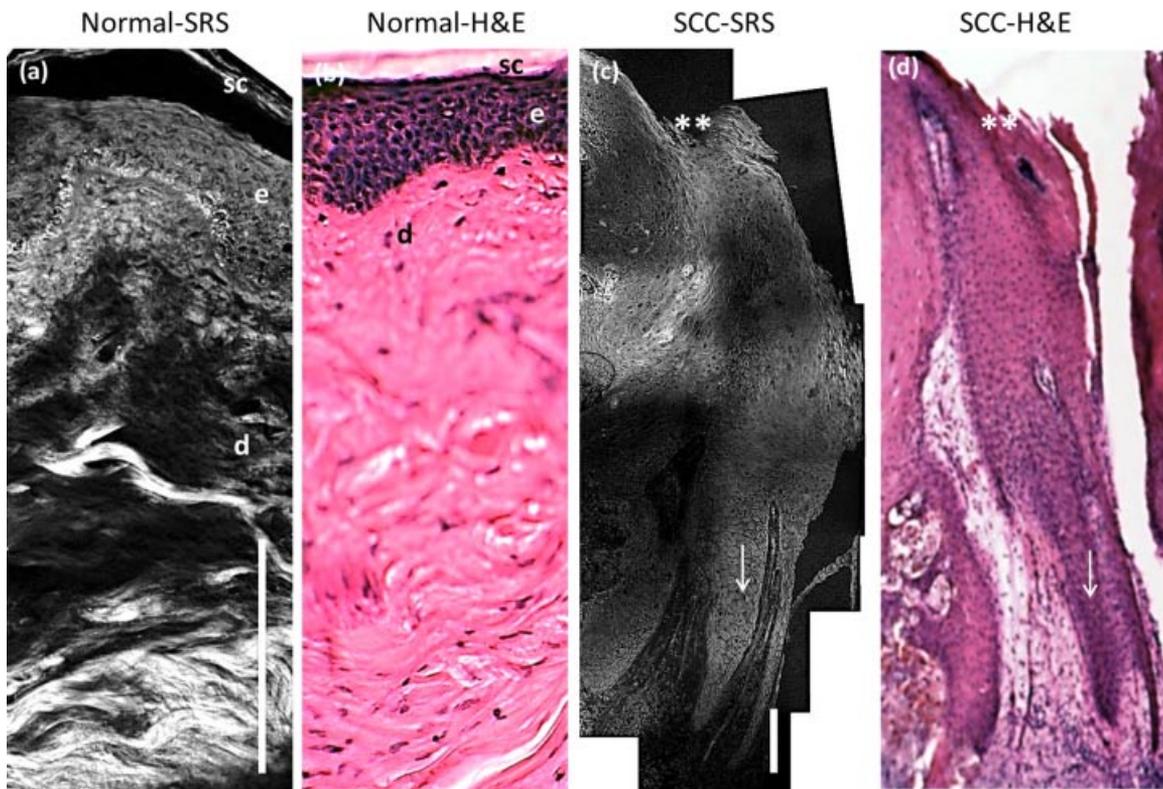

Fig. 3. Comparison of SRS mosaic images of healthy human skin and superficial SCC ex vivo. **a**: SRS unstained tissue image of healthy human skin. sc, stratum corneum; e, epidermis; d, dermis. **b**: H&E stained specimen of an adjacent healthy skin section. **c**: SRS unstained tissue image of superficial SCC. **d**: H&E stained specimen of an adjacent SCC section. ** marks the skin surface; arrow indicates the keratinocytes pushing into the dermis. The imaging anatomical depth of healthy and SCC sample is $300\,\mu m$ and 1.1 mm, respectively. Scale bar is $100\,\mu m$. Imaging performed using a 20X, 0.75NA Olympus objective lens.
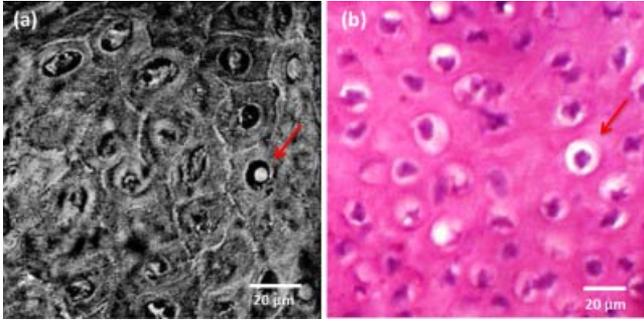
Fig. 4. Higher magnification image (60X, 1.2 NA water objective) of SCC tumor. **a**: SRS image of atypical cells in comparison with (**b**) H&E stained tissue. The arrow points to a single cell showing the signal from the cytoplasm and cell nuclei.

nuclei. Polymorphic and well differentiated cells as seen in the SRS images (Fig. 4a) represent a mildly atypical cell characteristic. The similarity between SRS and the H&E stained image is evident.

Figure 5a,b show SRS and H&E images of atypical keratinocytes that infiltrate into the dermis while still contained within the basement membrane. Randomly oriented keratinocytes with varying shapes and size that push into the dermis are clearly visualized. At higher magnification, a bright signal from the cell nucleus and the cytoplasm is observed in Figure 5e. Cell keratinization, the most significant feature of SCC, is readily mapped, owing to the sensitivity of the SRS technique to dense, kerati-

nized protein structures. Differentiated squamous epithelial cells with aggregated keratin are seen in Figure 5c. These features are in direct correspondence with the structures seen in the H&E stained tissue section (Fig. 5d). A strong protein signal from long keratin filaments is also visible using the SRS technique which remained unresolved in the H&E stained image (arrow marked in Figure 5 c,d).

DISCUSSION

In this study, the diagnostic qualities of SRS microscopy were examined relative to the RCM for the purpose of SCC identification. In addition, the features observed in SRS were compared to standard histopathology. The results of this study suggest that SRS provides more cellular details than seen in RCM, and that the cellular information correlates well with the diagnostic features of standard histopathology. In this study the SCC tissue was studied *ex vivo* to facilitate comparison with RCM and H&E. However, the ultimate utility of the SRS approach lies in its application *in vivo*. For this purpose, it is necessary to collect the SRS signal in the backscattered direction, a capability that was recently demonstrated for imaging *in vivo* [22]. In addition, clinical application of the SRS technique requires further miniaturization of the imaging system into a robust and flexible handheld device. In this regard, recent developments in endoscopic probe design indicate the feasibility of translating the SRS technique into clinically compatible instruments [23]. It should be noted that further miniaturization of the probe also offers
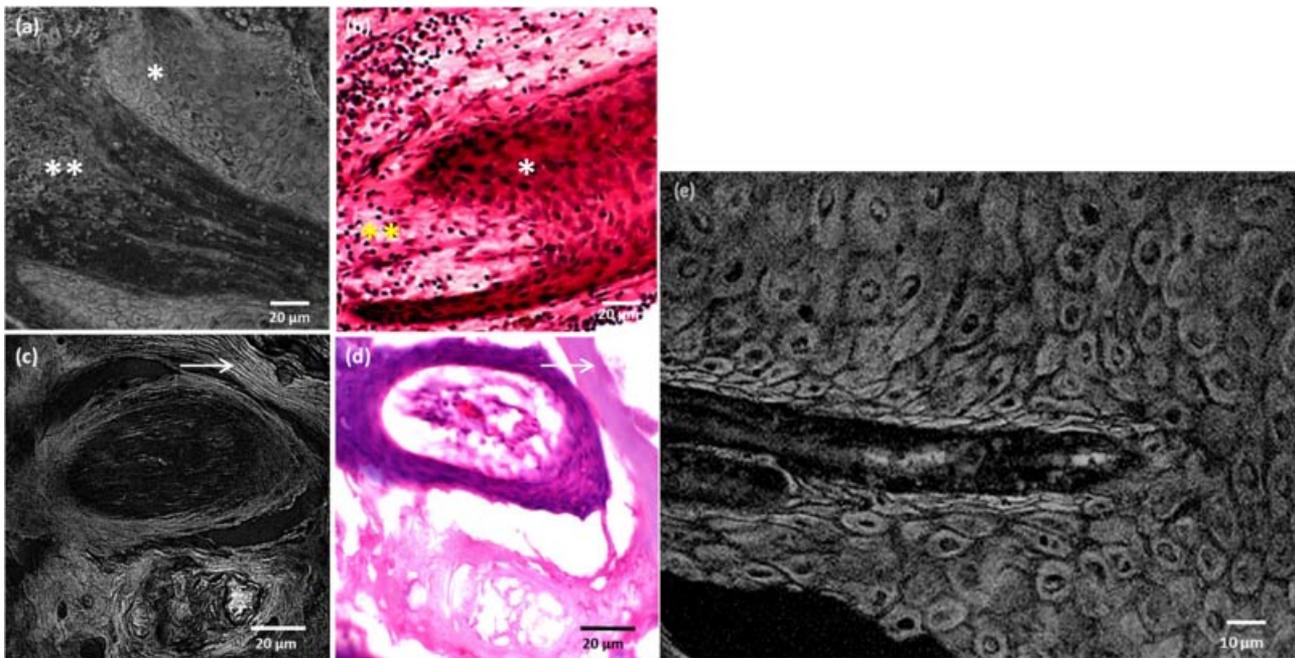

Fig. 5. Superficial SCC features as seen in SRS images in comparison with H&E image. **a**, **b**: Epidermal keratinocytes surrounding the dermis and (**c, d**) appearance of compact keratin as imaged using a 20X, 0.75NA objective. **e**: A zoom-in SRS image showing the tumor cells. Note the bright cellular and nuclear signal. * indicates the keratinocytes; ** indicates the dermis; arrow marks the keratin filaments.

opportunities for SRS examination of superficial tissues in hollow tracts of the human body, such as oral mucosa.

SRS contrast is based on Raman active molecular vibrations. Previously, spontaneous Raman microscopy studies have shown that differences in the Raman spectra of healthy and diseased skin can be used for detecting non-melanoma skin cancer [24–28]. However, conventional Raman spectroscopy is not suitable for rapidly generating high-resolution maps of skin tissue because of the long signal integration times. Instead, Raman spectroscopy is typically performed in a spatially averaged fashion, whereby morphological features are no longer resolved. Unlike Raman spectroscopy, the contrast in the SRS images is derived from a narrow spectral range. Yet, SRS images can be generated at acquisition rates that are clinically attractive. Moreover, SRS imaging resolves features that can be directly correlated to histopathological identifiers for SCC.

Reflectance confocal microscopy has been extensively studied as a possible tool for non-invasive skin imaging. Despite the simplicity, robustness and evolved clinical translation of RCM, its poor contrast yields limited subcellular details. Examination of important cellular features, such as nuclear size and shape, is difficult in RCM because of insufficient signal from nuclei relative to the surrounding cytoplasm. This has been resolved by externally washing the tissue with 5% acetic acid, which condenses the chromatin and brightens the cell nuclei [12–15]. This tissue treatment, however, reduces the ability to visualize the cell cytoplasm. Furthermore, RCM shows ill-defined tumor margins, which limits the ability to reliably differentiate the SCC from the surrounding tissue. To enhance contrast, RCM has been combined with fluorescence microscopy with the aid of suitable molecular contrast agents [16]. On the other hand, SRS images reveal the nuclear atypical cells and the cell keratinization without the application of labels.

The results of this study demonstrate that the specific histological properties of SCC previously identified through staining methods can be reproduced and visualized through non-invasive SRS imaging. Unlike staining methods, SRS imaging probes the molecular vibrations of chemical groups in endogenous compounds. It was previously shown that the ubiquitous presence of protein and lipids forms contrast akin to that seen in H&E stained tissue, and here we confirm the utility of this contrast for the case of SCC diagnosis. The ability to differentiate between healthy and cancerous skin tissue is demonstrated. A more challenging aspect for future investigation would be to explore SRS capability for diagnosing and mapping conditions such as AK and SCC *in situ*. Furthermore, with the development of an SRS fiber optic probe, real time imaging could be performed to guide the Mohs surgery.

Stimulated Raman scattering is a relatively new optical microscopy technique and despite its technical complexities has clear clinical potential. The cellular and nuclear features resolved in SRS imaging show more detail compared to similar features observed with confocal reflectance microscopy. The information content in SRS images is comparable to that in standard histopathology. This preliminary study provides an impetus for further, more comprehensive investigations to determine the diagnostic specificity and sensitivity of SRS for detecting skin cancers.

REFERENCES

1. Salasche SJ. Epidemiology of actinic keratoses and squamous cell carcinoma. J Am Acad Dermatol 2000;42(1 Pt 2):4.
2. Rogers H. Your new study of nonmelanoma skin cancers. Email to the skin cancer foundation March 31, 2010.
3. Squamous Cell Carcinoma. http://www.aad.org/skin-conditions/dermatology-a-to-z/squamous-cell-carcinoma. American Academy of Dermatology; August 27, 2012.
4. Zalaudek I, Argenziano G, Leinweber B, Citarella L, Hofmann-Wellenhof R, Malvehy J, Puig S, Pizzichetta M, Thomas L, Soyer H. Dermoscopy of Bowen's disease. Br J Dermatol 2004;150(6):1112–1116.
5. Braun RP, Rabinovitz HS, Oliviero M, Kopf AW, Saurat JH. Dermoscopy of pigmented skin lesions. J Am Acad Dermatol 2005;52(1):109–121.
6. Olmedo JM, Warschaw KE, Schmitt JM, Swanson DL. Optical coherence tomography for the characterization of basal cell carcinoma in vivo: A pilot study. J Am Acad Dermatol 2006;55(3):408–412.
7. Xu W, Ranger-Moore JR, Saboda K, Salasche SJ, Warneke JA, Alberts DS. Investigating sun-damaged skin and actinic keratosis with optical coherence tomography: A pilot study. Technol Cancer Res Treat 2003;2(6):525–535.
8. Rajadhyaksha M, Grossman M, Esterowitz D, Webb RH, Anderson RR. In vivo confocal scanning laser microscopy of human skin: Melanin provides strong contrast. J Invest Dermatol 1995;104(6):946–952.
9. Rajadhyaksha M, Anderson R, Webb RH. Video-rate confocal scanning laser microscope for imaging human tissues in vivo. Appl Opt 1999;38(10):2105–2115.
10. Rishpon A, Kim N, Porges L, Oliviero MC, Braun RP, Marghoob AA, Fox CA, Rabinovitz HS. Reflectance confocal microscopy criteria for squamous cell carcinomas and actinic keratoses. Arch Dermatol 2009;145(7):766.
11. Tannous Z, Torres A, González S. In vivo real-time confocal reflectance microscopy: A noninvasive guide for Mohs micrographic surgery facilitated by aluminum chloride, an excellent contrast enhancer. Dermatol Surg 2003;29(8):839–846.
12. Rajadhyaksha M, Menaker G, Flotte T, Dwyer PJ, GonzÃilez S. Confocal examination of nonmelanoma cancers in thick skin excisions to potentially guide mohs micrographic surgery without frozen histopathology. J Invest Dermatol 2001;117(5):1137–1143.
13. Chung VQ, Dwyer PJ, Nehal KS, Rajadhyaksha M, Menaker GM, Charles C, Jiang SB. Use of ex vivo confocal scanning

laser microscopy during Mohs surgery for nonmelanoma skin cancers. Dermatol Surg 2004;30(12p1):1470–1478.

14. Horn M, Gerger A, Koller S, Weger W, Langsenlehner U, Krippl P, Kerl H, Samonigg H, Smolle J. The use of confocal laser-scanning microscopy in microsurgery for invasive squamous cell carcinoma. Br J Dermatol 2007;156(1):81–84.

15. Patel YG, Nehal KS, Aranda I, Li Y, Halpern AC, Rajadhyaksha M. Confocal reflectance mosaicing of basal cell carcinomas in Mohs surgical skin excisions. J Biomed Opt 2007;12(3): 034027.

16. Al-Arashi MY, Salomatina E, Yaroslavsky AN. Multimodal confocal microscopy for diagnosing nonmelanoma skin cancers. Lasers Surg Med 2007;39(9):696–705.

17. Paoli J, Smedh M, Wennberg AM, Ericson MB. Multiphoton laser scanning microscopy on non-melanoma skin cancer: Morphologic features for future non-invasive diagnostics. J Invest Dermatol 2007;128(5):1248–1255.

18. Skala MC, Squirrell JM, Vrotsos KM, Eickhoff JC, Gendron-Fitzpatrick A, Eliceiri KW, Ramanujam N. Multiphoton microscopy of endogenous fluorescence differentiates normal, precancerous, and cancerous squamous epithelial tissues. Cancer Res 2005;65(4):1180–1186.

19. Freudiger CW, Min W, Saar BG, Lu S, Holtom GR, He C, Tsai JC, Kang JX, Xie XS. Label-free biomedical imaging with high sensitivity by stimulated Raman scattering microscopy. Science 2008;322(5909):1857–1861.

20. Ploetz E, Laimgruber S, Berner S, Zinth W, Gilch P. Femtosecond stimulated Raman microscopy. Appl Phys B 2007;87(3):389–393.

21. Freudiger CW, Pfannl R, Orringer DA, Saar BG, Ji M, Zeng Q, Ottoboni L, Ying W, Waeber C, Sims JR. Multicolored stain-free histopathology with coherent Raman imaging. Lab Invest 2012;92(10):1492–1502.

22. Saar BG, Freudiger CW, Reichman J, Stanley CM, Holtom GR, Xie XS. Video-rate molecular imaging in vivo with stimulated Raman scattering. Science 2010;330(6009):1368–1370.

23. Saar BG, Johnston RS, Freudiger CW, Xie XS, Seibel EJ. Coherent Raman scanning fiber endoscopy. Opt Lett 2011; 36(13):2396.

24. Lieber CA, Majumder SK, Billheimer D, Ellis DL, Mahadevan-Jansen A. Raman microspectroscopy for skin cancer detection in vitro. J Biomed Opt 2008;13(2): 024013.

25. Lieber CA, Majumder SK, Ellis DL, Billheimer DD, Mahadevan-Jansen A. In vivo nonmelanoma skin cancer diagnosis using Raman microspectroscopy. Lasers Surg Med 2008; 40(7):461–467.

26. Caspers P, Lucassen G, Puppels G. Combined in vivo confocal Raman spectroscopy and confocal microscopy of human skin. Biophys J 2003;85(1):572–580.

27. Gniadecka M, Wulf HC, Nielsen OF, Christensen DH, Hercogova J. Distinctive molecular abnormalities in benign and malignant skin lesions: Studies by Raman spectroscopy. Photochem Photobiol 1997;66(4):418–423.

28. Zhao J, Lui H, McLean DI, Zeng H. Real-time Raman spectroscopy for non-invasive skin cancer detection-preliminary results. IEEE. 2008; p 3107–3109.